

Mesoscopic CH₃NH₃PbI₃/TiO₂ heterojunction solar cells.

Lioz Etgar^{1*}, Gao Peng¹, Zhaosheng Xue², Bin Liu², Md K. Nazeeruddin¹, Michael Grätzel¹

¹ Laboratoire de Photonique et Interfaces, Institut des Sciences et Ingénierie Chimiques, École Polytechnique Fédérale de Lausanne (EPFL), Switzerland.

² Department of Chemical and Biomolecular Engineering, National university of Singapore, Singapore.

ABSTRACT: We report for the first time on a hole conductor-free mesoscopic lead iodide CH₃NH₃PbI₃(perovskite)/TiO₂ heterojunction solar cell, produced by deposition of perovskite nanoparticles from a solution of CH₃NH₃I and PbI₂ in γ -butyrolactone on a 400nm thick film of TiO₂ (anatase) nanosheets exposing (001) facets. An Au film was evaporated on top of the CH₃NH₃PbI₃ served as a back contact. Importantly, the CH₃NH₃PbI₃ nanoparticles act as hole conductor simultaneously the role of light harvester and hole conductor rendering superfluous the use of an additional hole transporting material. The simple mesoscopic CH₃NH₃PbI₃/TiO₂ heterojunction solar cell shows impressive photovoltaic performance with short circuit photocurrent (J_{sc}) of 16.1 mA/cm², an open circuit photovoltage (V_{oc}) of 0.631 V and a fill factor (FF) of 0.57, corresponding to a light to electric power conversion efficiency (PCE) of 5.5% under standard AM 1.5 solar light of 1000 W/m² intensity. At a lower light intensity of 100W/m² a PCE of 7.3 % was measured. The advent of such simple solution processed mesoscopic heterojunction solar cells paves the way for new advances to realize low cost, high-efficiency solar cells.

Introduction

Due to their large optical cross section nanocrystalline pigments are attractive light harvesters in solar conversion systems. In particular quantum dots (QDs) have attracted a lot of attention due to their tunable band gap.¹⁻³ A variety of strategies have been applied to integrate QDs into solar cells, including QD-polymer hybrid solar cells, QD-Schottky barrier solar cells, QD-sensitized titanium dioxide (TiO₂) solar cells, and QD hybrid bilayer solar cells.⁴⁻¹² Re-

cent investigations focus on depleted heterojunction devices, employing a mesoscopic wide band gap semiconductor oxide such as TiO₂ or ZnO as a thin spacer layer between the QDs and the conducting transparent oxide current collector.¹³⁻²¹ Efficiencies of 5-6% were observed with these simple structures. In addition, a tandem QDs solar cell with the same structure has been demonstrated as well.¹⁸ Multiple exciton generation (MEG) effect was also demonstrated in similar QDs based solar cell structure.^{22,23} While such heterojunction QD solar cells show promising photovoltaic performance, they still are facing problems such as stability, low open circuit voltage and fast carrier recombination which prevent them from achieving higher efficiencies.

The direct band gap, large absorption coefficients^{24,25} and high carrier mobility^{26,27} of organo-lead halide perovskites render them very attractive for use as light harvesters in mesoscopic hetero-junction solar cells. Their electronic properties can be tailored using the organic component allowing e.g. for layered materials to be formed where the distance and the electronic coupling between the inorganic sheets can be controlled by the structure of the organic component. The layered perovskite have high stability in dry air.

Importantly these perovskites nanopigments are easy to prepare and simple to deposit by solution processing such as spin- or dip coating. The perovskite precipitates from a solution of PbI₂ and methylammonium iodide forming CH₃NH₃PbI₃ crystals within the pores and on the surface of the mesoscopic TiO₂ substrate. The ionic and covalent interaction between the metal cations and the halogen anions creates inorganic octahedra, while the cationic alkylammonium head groups bind to the halogens to charge balance the structure. Previous reports used CH₃NH₃PbI₃ nanocrystals as sensitizers in pho-

toelectrochemical cells with liquid electrolyte^{28,29,30}. However the performance of these systems rapidly declined due to dissolution of the perovskite. Very recently, the tin iodide based perovskite CsSnI₃ has been employed as a hole conductor along together with N719 as sensitizer in solid state dye-sensitized solar cells yielding a PCE of 8.5%.³¹

Here we report on CH₃NH₃PbI₃ perovskite/TiO₂ heterojunction solar cell using anatase nanosheets with dominant (001) facets as electron collector. The perovskite act as an absorber and at the same time as a hole conductor, rendering superfluous the use of an additional p-type material for transporting positive charge carriers. This simple mesoscopic heterojunction solar cell achieved a remarkable photovoltaic performance with current density of 16.1 mA cm⁻², FF of 0.57 and Voc of 0.631V corresponding to a light to electric power conversion efficiency (PCE) of 5.5% under 1 sun intensity. This is the first report on the successful use of CH₃NH₃PbI₃ as an absorber and hole transporting material in a heterojunction solar cell.

Results and discussion

The synthesis of CH₃NH₃PbI₃ and deposition on the mesoporous TiO₂ film was carried out by spin coating a 40 wt% precursor solution of CH₃NH₃I and PbI₂ in γ -butyrolactone. CH₃NH₃I was synthesized by reaction of HI with 40% methylamine in methanol solution and recrystallization. The film coated on the TiO₂ darkened upon drying at room temperature, indicating the formation of CH₃NH₃PbI₃ in the solid state.

Figures 1A and 1B present a scheme of the device structure and its energy level diagram. The conduction and valence bands of the CH₃NH₃PbI₃ permit electron injection and hole transportation to the TiO₂ and the gold respectively. The bottom part of the device, acting as electron collector, is composed of a 100 nm thick hole blocking compact TiO₂ film supported by the FTO transparent glass front contact, onto which a ca 500 nm thick layer of the TiO₂ nanosheets was deposited. The light is absorbed by the CH₃NH₃PbI₃ nanoparticles, which were deposited onto the TiO₂ by spin coating technique. A gold contact was evaporated on top of the CH₃NH₃PbI₃ thin film.

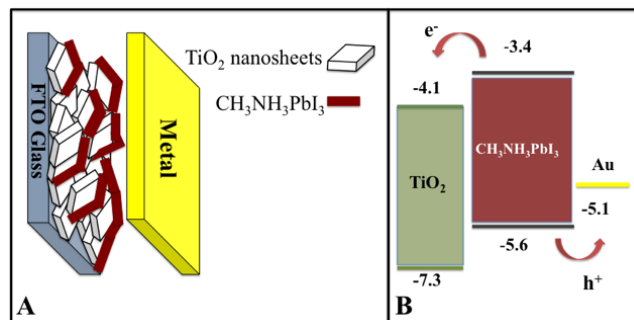


Figure 1 : (A) Scheme of the device structure ; (B) Energy level diagram of the CH₃NH₃PbI₃/TiO₂ heterojunction solar cell.

Figure 2 shows high resolution scanning electron microscopy (HR-SEM) image of the cross section of the solar cell. The change in contrast above the compact TiO₂ layer indicates the penetration of the CH₃NH₃PbI₃ nanocrystals into the pores formed by the anatase film.

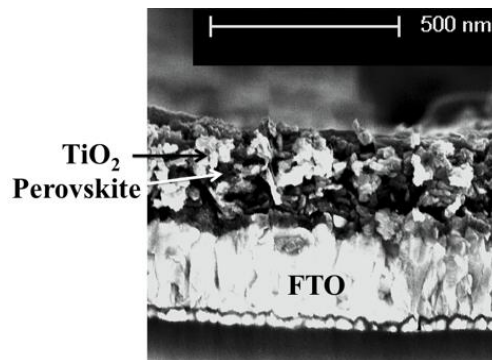


Figure 2 : Transmission electron microscopy picture of the cross section of the CH₃NH₃PbI₃/TiO₂ heterojunction solar cell. The dark areas can be attributed to the CH₃NH₃PbI₃ which penetrates through the mesopores TiO₂ film.

Figure 3A exhibits J-V characteristics of the mesoscopic CH₃NH₃PbI₃/TiO₂ heterojunction photovoltaic cell under 1 sun illumination. Under standard reporting conditions, i.e. AM 1.5 solar light at 1000 W/m² the device produced an open-circuit voltage (V_{oc}) of 0.631 V, a short circuit current density (J_{sc}) of 16.1 mA cm⁻² and a fill factor of 57% corresponding to a power conversion efficiency (PCE) of 5.5% (table 1). The PCE increase at 100 W/m² intensity to 7.28% with J_{sc} of 2.14 mA cm⁻², a fill factor of 62% and Voc of 0.565 V.

The incident photon to current conversion efficiency (IPCE) specifies the ratio of extracted electrons to incident photons at a given wavelength. The IPCE spectrum (Figure 3B) is plotted as a function of wavelength of the light. The solid state

CH₃NH₃PbI₃/TiO₂ heterojunction solar cell shows an excellent response from 400 - 800nm, the IPCE is reaching its maximum of 90% over the wavelength range from 400 nm to 540 nm decreasing at longer wavelength till 780nm. Integration of the IPCE spectrum over the AM1.5 solar emission yields a photocurrent density of 16.2 mA/cm², in good agreement with the measured values, showing that the spectral mismatch between the solar simulator employed and the true AM 1.5 solar emission is negligibly small.

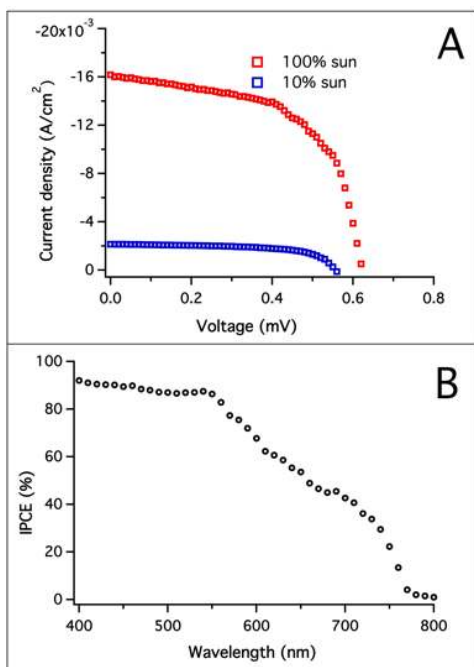


Figure 3: (A) J-V characteristic of the Lead iodide Perovskite/TiO₂ heterojunction solar cell; (B) IPCE spectrum of the device.

Table 1: Photovoltaic device parameters of the CH₃NH₃PbI₃/TiO₂ solar cell

Sun Intensity	Jsc (mA/cm ²)	Voc (mV)	FF	P (%)
10	2.1	565.8	0.62	7.28
100	16.1	631.6	0.57	5.5

Conclusions

In summary the present work establishes for the first time that CH₃NH₃PbI₃ nanocrystals can act both as efficient light harvester and hole transporter in solar cells comprising a meoscopic

CH₃NH₃PbI₃/TiO₂ heterojunction. The role of the TiO₂ nanoplatelets is to accept electrons and transport them to the front collector. This eliminates the need for employing an additional organic or inorganic hole conductor, whose infiltration in the mesoporous TiO₂ has posed difficulties in the past. There is much room for further improvement of the PCE in particular by increasing the FF and Voc and this will be the focus of our continuing investigations. The fact that the perovskite is stable in dry ambient air and can be deposited by low cost solution processing opens up new ways for future development of high efficiency low cost photovoltaic cells.

Experimental

CH₃NH₃I synthesis

CH₃NH₃I was synthesized by reacting 30 mL methylamine (40% in methanol, TCI) and 32.3 mL of hydroiodic acid (57 wt% in water, Aldrich) in a 250 mL round bottomed flask at 0 °C for 2 h with stirring. The precipitate was recovered by putting the clear solution on a roti-vapor and carefully removed the solvents at 50 °C. The yellowish raw product, methylammonium iodide (CH₃NH₃I), was washed with diethyl ether by stirring the solution for 30 min, which was repeated three times, and then finally recrystallized from a mixed solvent of diethyl ether and ethanol. After filtration, the solid was collected and dried at 60 °C in vacuum oven for 24 h.

Synthesis and purification of TiO₂ nanosheets

The synthesis of the nanosheets followed the typical experimental procedure. ³²Ti(OBu)₄ (10 mL, 98%) and hydrofluoric acid (0.8 mL, 47%) solution mixed in a 150 mL dried Teflon autoclave which was kept at 180 °C for 24 h to yield well-defined rectangular sheet-like structures with a side length of 30 nm and a thickness of 7 nm. After the reaction the dispersion was cooled to room temperature, the white powder was separated by high-speed centrifugation and washed with ethanol followed by distilled water for several times.

Caution: Hydrofluoric acid is extremely corrosive and a contact poison, it should be handled with extreme care! Hydrofluoric acid solution is stored in Teflon containers in use.

Solar cell fabrication

Thin dense TiO₂ layer of ~100 nm thickness was deposited onto a SnO₂:F conducting glass substrate (15Ω/cm, Pilkington) by spray pyrolysis method³³. The deposition temperature of TiO₂ compact layer was 450 °C. TiO₂ nanosheet films of ~0.5 μm thickness was prepared by spin coating method onto this

substrate using the TiO₂ nanosheets with 001 dominant facets. The TiO₂ layer was annealed at 500 °C for 30 min in air. The substrate was immersed in 40 mM TiCl₄ aqueous solutions for 30 min at 70 °C and washed with distilled water and ethanol, followed by annealing at 500 °C for 30 min in air.

The synthesis of CH₃NH₃PbI₃ on the TiO₂ surface was carried out by dropping on the TiO₂ film a 40 wt% precursor solution of equimolar CH₃NH₃I and PbI₂ in γ -butyrolactone. Film formation by spin coating (2000 rpm, 30 sec) in the glove box.

The film coated on the TiO₂ changed its color upon drying at room temperature, indicating the formation of CH₃NH₃PbI₃ in the solid state. The CH₃NH₃PbI₃ film was annealed under argon for 15min at 100°C.

Finally the counter electrode was deposited by thermal evaporation of gold under a pressure of 5×10^{-5} Torr. The active area was 0.12 cm². After the preparation, the cells were allowed to expose in air.

Photovoltaic Characterization

Photovoltaic measurements employed an AM 1.5 solar simulator equipped with a 450W xenon lamp (Model No. 81172, Oriel). Its power output was adjusted to match AM 1.5 global sunlight (100 mW/cm²) by using a reference Si photodiode equipped with an IR-cutoff filter (KG-3, Schott) in order to reduce the mismatch between the simulated light and AM 1.5 (in the region of 350–750 nm) to less than 2% with measurements verified at two PV calibration laboratories [ISE (Germany), NREL (USA)]. I–V curves were obtained by applying an external bias to the cell and measuring the generated photocurrent with a Keithley model 2400 digital source meter. The voltage step and delay time of photocurrent were 10 mV and 40 ms, respectively. A similar data acquisition system was used to determine the monochromatic incident photon-to-electric current conversion efficiency. Under full computer control, light from a 300 W xenon lamp (ILC Technology, U.S.A.) was focused through a Gemini-180 double monochromator (Jobin Yvon Ltd., U.K.) onto the photovoltaic cell under test. The monochromator was incremented through the visible spectrum to generate the IPCE (λ) as defined by $IPCE(\lambda) = 12400(J_{sc}/\lambda\phi)$, where λ is the wavelength, J_{sc} is short-circuit photocurrent density (mA cm⁻²), and ϕ is the incident radiative flux (mW cm⁻²). Photovoltaic performance was measured by using a metal mask with an aperture area of 0.49 cm². The cross section of the device was measured by Zeiss Jemini FEG-SEM, using 5kV with magnification of 250KX.

AUTHOR INFORMATION

Corresponding Author

Dr. Lioz Etgar, email: lioiz.etgar@epfl.ch

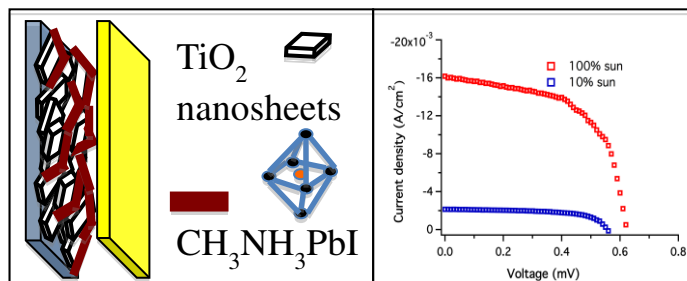
Funding Sources

No competing financial interests have been declared.

ACKNOWLEDGMENT

This work was partially supported by EU FP7 project ENERGY-261920 “ESCORT”. M.K.N. thanks the World Class University program, Photovoltaic Materials, Department of Material Chemistry, Korea University, Chungnam, 339-700, Korea, funded by the Ministry of Education, Science and Technology through the National Research Foundation of Korea (No. R31-2008-000-10035-0).

Table of Contents



REFERENCES

- ¹ Huynh, W. U.; Dittmer, J. J.; Alivisatos, A. P. *Science* **2002**, 295, 2425.
- ² I. Gur, N.; A. Fromer, M. I Geier; A. P Alivisatos. *Science* **2005**, 310, 462.
- ³ W. J. E. Beek,; M. M Wienk; R. A. J. Janssen. *Adv. Func. Mater* **2006**, 16, 1112.
- ⁴ J. M. Luther; M. Law; M. C. Beard; Q. Song; M. O. Reese; R. J. Ellingson; A. J. Nozik. *Nano lett.* **2008**, 8, 3488.
- ⁵ W. Ma; J. M. Luther; H. Zheng; Y. Wu; A. P. Alivisatos. *Nano lett.* **2009**, 9, 1699.
- ⁶ R. Plass; S. Pelet; J. Krueger; M. Grätzel; U. Bach. *J. Phys. Chem. B*, **2002**, 106, 7578.
- ⁷ B. Sun; A. T. Findikoglu; M. Sykora; D. J. Werder; V. I. Klimov. *Nano lett.* **2009**, 9, 1235.
- ⁸ J. M. Luther; M. Law; Q. Song; C. L. Perkins; M. C. Beard; A. J. Nozik. *ACS Nano*, **2008**, 2, 271.
- ⁹ S. Zhang; P. W. Cyr; S. A. McDonald; G. Konstantatos; E. H. Sargent. *Appl. Phys. Lett.* **2005**, 87, 233101.
- ¹⁰ B.-R. Hyun; Y.-W. Zhong; A. C. Bartnik; L. Sun, H. D. Abruña; F. W. Wise; J. D. Goodreau; J. R. Matthews; T. M. Leslie; F. Borrelli. *ACS Nano*, **2008**, 2, 2206.
- ¹¹ D. Ratan; T. Jiang; D. A. Barkhouse; W. Xihua; G. P.-A. Andras; B. Lukasz; L. Larissa; E. H. Sargent. *J. Amer. Chem. Soc.* **2010**, 132, 5952.
- ¹² J. M. Luther; J. Gao; M. T. Lloyd; O. E. Semonin; M. C. Beard; A. J. Nozik. *Adv. Mater.* **2010**, 22, 3704.
- ¹³ A. G. Pattantyus-Abraham; I. J. Kramer; A. R. Barkhouse; X. Wang; G. Konstantatos; R. Debnath; L. Levina; I. Raabe; M. K. Nazeeruddin; M. Gratzel; E. H. Sargent. *ACS Nano*. **2010**, 4(6), 3374.
- ¹⁴ H. Liu; J. Tang; I. J. Kramer; R. Debnath; G. I. Koleilat; X. Wang; A. Fisher; R. Li; L. Brzozowski; L. Levina; E. H. Sargent. *Adv. Mater.* **2011**, 23, 3832.
- ¹⁵ J. Gao; J. M. Luther; O. E. Semonin; R. J. Ellingson; A. J. Nozik; M. C. Beard. *Nano Lett.* **2011**, 11 (3), pp 1002.
- ¹⁶ J. Gao; C. L. Perkins; J. M. Luther; M. C. Hanna; H. Y. Chen; O. E. Semonin; A. J. Nozik; R. J. Ellingson; M. C. Beard. *Nano Lett.* **2011**, 11 (8), pp 3263.
- ¹⁷ D. A. R. Barkhouse; R. Debnath; I. J. Kramer; D. Zhitomirsky; A. G. Pattantyus-Abraham; L. Levina; L. Etgar; M. Grätzel; Edward H. Sargent. *Adv. Mater.* **2011**, 23, 3134.
- ¹⁸ X. Wang; G. I. Koleilat; J. Tang; H. Liu; I. J. Kramer; R. Debnath; L. Brzozowski; D. A. R. Barkhouse; L. Levina; S. Hoogland; E. H. Sargent. *Nature photonics* **2011**, 5, 480.
- ¹⁹ K. S. Leschikies; T. J. Beatty; M. S. Kang; D. J. Norris; E. S. Aydil. *ACS Nano* **2009**, 3(11), 3638.
- ²⁰ Lioz Etgar; Wei Zhang; Stefanie Gabriel; Stephen G. Hickey; Md K. Nazeeruddin; Alexander Eychmüller; Bin Liu; Michael Grätzel. *Advanced Materials* **2012**, 24(16), 2202-2206.
- ²¹ Lioz Etgar; Thomas Moehl; Stefanie Tschardtke; Stephen G. Hickey; Alexander Eychmüller and Michael Grätzel. *ACS Nano* **2012**, 6 (4), 3092-3099.
- ²² J. B. Sambur; T. Novet; B. A. Parkinson. *Science* **2010**, 330, 63.
- ²³ O. F. Semonin; J. M. Luther; S. Choi; H. Y. Chen; J. Gao; A. J. Nozik; M. C. Beard. *Science* **2011**, 334, 1530.
- ²⁴ Akihiro Kojima; Masashi Ikegami; Kenjiro Teshima; and Tsutomu Miyasaka. *Chem. Lett.* **2012**, 41, 397.

-
- ²⁵ C. I. Covaliu; L. C. Chioaru; L. Craciun; O. Oprea; I. Jitaru. *Optoelectronics and advanced materials* **2011**, 5 (10), 1097.
- ²⁶ C.R. Kagan ; D. B. Mitzi ; C. D. Dimitrakopoulos. *Science* **286**, 945, 1999.
- ²⁷ D.B Mitzi ; C.A. Feild ; Z. Schlesinger ; R.B. Laibowitz ; *J.Solid State Chem.* **1995**, 114, 159.
- ²⁸ Akihiro Kojima; Kenjiro Teshima ; Yasuo Shirai; Tsutomu Miyasaka. *J.Am. Chem. Soc.* **2009**, 131, 6050–6051.
- ²⁹ Jeong-Hyoek Im; Jaehoon Chung; Seung-Joo Kim; Nam-Gyu Park. *Nanoscale Research Letters*, **2012**, 7, 353.
- ³⁰ Jeong-Hyeok Im; Chang-Ryul Lee; Jin-Wook Lee; Sang-Won Park; Nam-Gyu Park. *Nanoscale* **2011**, 3, 4088.
- ³¹ Chung, I.; Lee, B.; He, J.; Chang, R. P. H.; Kanatzidis, M. G. *Nature* **2012**, 485, 486-489.
- ³² X. Han; Q. Kuang; M. Jin; Z. Xie; L. Zheng. *J. Am. Chem. Soc.* **2009**, 131 (9), 3152.
- ³³ Moon, S. J.; Yum, J. H.; Humphry-Baker, R.; Karlsson; K. M.; Hagberg, D. P.; Marinado, T.; Hagfeldt, A.; Sun, L. C.; Grätzel, M.; Nazeeruddin, M. K. *J. Phys. Chem. C* **2009**, 113, 16816.